Applied Ocean Research 138 (2023) 103679

Contents lists available at ScienceDirect

Applied Ocean Research

journal homepage: www.elsevier.com/locate/apor

Experimental ultimate strength assessment of stiffened plates subjected to marine immersed corrosion

Krzysztof Woloszyk [a], Yordan Garbatov [b,*], Jakub Kowalski [a]

[a] Institute of Naval Architecture, Gdansk University of Technology, G. Narutowicza 11/12 st., Gdansk 80-233, Poland
[b] Centre for Marine Technology and Ocean Engineering (CENTEC), Instituto Superior Técnico, Universidade de Lisboa, Avenida Rovisco Pais, Lisboa 1049-001, Portugal

ARTICLE INFO

Keywords:
Corrosion
Ultimate strength
Stiffened plate
Experiment

ABSTRACT

This study experimentally analyses the impact of marine immersed corrosion degradation on the compressive strength of the stiffened plates where the lower degradation levels were considered. The corrosion degradation test was accelerated by controlling the natural corrosion environmental factors, avoiding applying an electric current. Different groups of corrosion degradation levels and initial plate thicknesses were investigated. The specimens were subjected to a compressive load via a universal testing machine. The estimated force-displacement relationships and lateral displacements as a function of the degree of degradation were analysed. Several analyses and discussions showed that considering only the mean value of the corrosion thickness loss, it is insufficient to evaluate the stiffened plates' ultimate strength correctly, and the type of corrosion degradation needs to be accounted for appropriately.

1. Introduction

Corrosion degradation is one of the main ageing effects that need to be considered when analysing the structural response of ageing ships and offshore structures. The corrosion degradation may significantly deteriorate the load-carrying capacity and structural integrity (Bai and Jin, 2016; Guedes Soares et al., 2008; Melchers, 2008), primarily due to the reduction of plate thickness, surface roughness leading to the development of surface stress concentrations (Kodvanj et al., 2021) and accelerated fatigue damage (Garbatov et al., 2014a), material properties changing (Garbatov et al., 2014b), etc. Two main corrosion types could be distinguished, i.e. general and pitting (Wang et al., 2014). The general corrosion may result in the non-uniform reduction of plate thickness, whereas pitting corrosion results in localised pits observed within the structural components (Zayed et al., 2018). The corrosion structural degradation depends on the location of the structural component and its orientation, the physical and chemical characteristics of the complex corrosion environment.

The ship-side shell structures are subjected to different upper (atmospheric) intermediate (splash) and lower (immersed) zone environments (Zayed et al., 2018). The upper (zone) ship-side shell is subjected to a severe atmospheric environment, defined by the rich content of chloride, oxygen, and other corrosive driven compounds. In this zone, the ship deck structure is subjected to corrosion degradation due to the green water, rain, and water collection, including the high humidity and oxygen accelerated by the aggressive marine environment. The seawater spray rising from the ship motion and wave effects on deck structures additionally contribute to the corrosion degradation. The lower zone of the ship-side shell is fully immersed in seawater. The water properties such as salinity, temperature, oxygen content, pH level and chemical composition can vary according to the ship's location in the ocean. The water flow accelerates the corrosion degradation because it removes the corrosion rust layer and re-exposes the base metal to the corrosive, aggressive environment, keeping the degradation at a high level. The splash ship-side shell zone is subjected to a highly aggressive corrosive environment. The structures are continuously aerated because of the seawater surface turbulence, leading to increased oxygen contents and the wear effects of ship motion, including the wet and dry development.

The marine immersed and splash zone corrosion degradation were compared in (Zhang et al., 2017), where different mechanisms governing the corrosion degradation and different surface morphologies were identified. It was found that depending on the corrosion type, the corrosion rate will be different, including the corrosion degradation characteristics and material properties of the corroded structural components. Further, the atmospherically corroded specimens (Wang et al., 2017) were shown to have other corrosion degradation characteristics

* Corresponding author.
E-mail address: yordan.garbatov@tecnico.ulisboa.pt (Y. Garbatov).

https://doi.org/10.1016/j.apor.2023.103679
Received 30 December 2021; Received in revised form 30 March 2022; Accepted 24 July 2023
Available online 28 July 2023

compared to those corroded in immersed conditions (Woloszyk et al., 2021b). In the first case, the lower or higher corrosion diminutions regions are smaller than in the second case. Different corrosion characteristics will impact the structural response of corroded components (Woloszyk and Garbatov, 2020a).

The most commonly used method is to accelerate the process of corrosion testing by application of electric current. However, corrosion degradation type will be important, but its acceleration in laboratory conditions during the corrosion testing is also important. The surface characteristics will be different from the naturally accelerated corrosion degradation as found in Xiao et al. (2020), Yuan et al. (2007). Thus, it is crucial to investigate the structural response of corroded components with a specified type of corrosion and the method of its acceleration.

The experimental study presented here deals with ship structural components subjected to immersed corrosion degradation. The corrosion degradation is experimentally developed by controlling the most critical governing parameters that have been already discussed in Woloszyk et al. (2021b), Woloszyk and Garbatov (2021).

The research related to the ultimate strength of corroded structural members was carried out using numerical and experimental approaches analysing different complexity of structures like plate, stiffened plates, and box structures. The most basic structural components are unstiffened plates. The numerical investigations of the ultimate strength of compressed corroded plates were carried out, applying uniform (Guedes Soares and Garbatov, 1999; Mateus and Witz, 1998) and non-uniform corrosion models (Rahbar-Ranji, 2012; Reza Khedmati et al., 2011; Woloszyk et al., 2018; Woloszyk and Garbatov, 2020b). The observed strength reduction was significant, but non-uniform corrosion models predicted higher capacity reduction than uniform models. The strength reduction varied between different studies of similar corroded structural components, which can be explained, additionally to many other factors, to the non-specified corrosion degradation environment.

The second most fundamental structural component in ship structures that resist compressive longitudinal loads is the stiffened plates, composed of a longitudinal stiffener with attached plating. There are spanned between the very rigid transverse frames. The most crucial structural elements are those located near the bottom and the deck of the ship. Investigating the ultimate strength of both structural components allows for predicting the ultimate strength of the ship hull girder providing information about factors governing the strength and structural behaviour. A significant decrease in the ultimate strength of stiffened plates with different corrosion degradation levels was observed in experiments performed by Garbatov et al. (2017). The stiffened plates were taken from the box girder, corroded in natural marine conditions accelerated by applying electric current (Domzalicki et al., 2009).

Further, the numerical model employing the combined effect of the uniform thickness loss and subsequent mechanical properties reduction was developed by Woloszyk et al. (2018), showing excellent agreement with the experimental results presented in Garbatov et al. (2017). Unfortunately, the degree of degradation levels was very high in that case (above 40%), and experiments on structural components with lower levels of corrosion degradation are lacking. In-service life, a significant corrosion degradation level is not allowed, and structural components are replaced. Other studies related to corroded stiffened plates and panels' ultimate strength could be found in Kim et al. (2012a), Mohammad et al. (2010).

Saad-Eldeen et al. (2014, 2013, 2011) performed a series of four-point bending moment tests of corroded box girders. Similarly to Garbatov et al. (2017), the corrosion was generated in a real seawater condition, but it was accelerated by applying an electric current (Domzalicki et al., 2009). In this case, the reduction of box girders' structural capacity was significant too. Additionally, the observed structural behaviour was asymmetrical due to the uneven distribution of thickness within the specimens. Based on experimental results and dimensional theory, the prediction of the ultimate strength of a real-scale ship hull was performed in Garbatov et al. (2015). The review of the corrosion degradation and damage impact on the ageing ship hull structures was shown in Tekgoz et al. (2020), Wang et al. (2009), where the results of many other studies were analysed. The observed ship hull girder section modulus loss varies from 4% to 20%, mainly due to the assumptions and models used in the analysis. Some studies related to that problem may be found in Kim et al. (2012b), Vu and Dong (2020), Vu Van and Yang (2017).

The present work aims to analyse the ultimate strength of corroded stiffened plates. The specimens made of normal strength steel of three different thicknesses are subjected to marine immersed corrosion degradation, simulated in laboratory conditions (Woloszyk et al., 2021b). Only natural governing factors of the corrosion environment are controlled, avoiding accelerating the process with the application of electric current. The experiments in such corrosion environmental conditions were not performed in previous research works. Further, the stiffened plates are subjected to a compressive load, and all relevant data are recorded, i.e., force-displacement relationships, lateral displacements, and post-collapse behaviours. The ultimate strength is compared with the available empirical formulations, showing that the mean value thickness reduction is insufficient to evaluate the impact of corrosion degradation on the ultimate strength of stiffened plates.

2. Corrosion degradation and experimental set-up

The stiffened plates of various initial thicknesses, namely 5, 6 and 8 mm, are analysed. The specimens are composed of a 1.25 m long and 0.4 m wide plate, and the attached flat-bar stiffener is 0.1 m in height. The plate and the stiffener were of the same thickness for each specimen. They were made of typical shipbuilding steel of normal strength with a nominal yield strength of 235 MPa. The initial material properties were determined based on the tensile test of several coupon specimens, as reported in Woloszyk et al. (2020) and presented in Table 1.

From each thickness, four specimens were fabricated. A total of three specimens were tested in intact non-corroded conditions, and the testing results were presented in Woloszyk et al. (2020). In contrast, nine specimens were subjected to accelerated corrosion testing. The automatic arc-welding has been adopted to ensure similar post-welding residual stresses and deflections, leading to identical welding parameters for each group of thicknesses. The measurements of the post-welding residual stresses have also been discussed in Woloszyk et al. (2020), showing a relatively low level compared to the ones found in the literature. The post-welding deflections were measured using the photogrammetry technique before the corrosion process, as presented in Woloszyk et al. (2021a). Since there are caused by the welding process, the corrosion will not have an impact on the shape or size of imperfections. The general shape of specimens is presented in Fig. 1 and values of measured imperfections are given in Table 2. The negative values denote that the imperfection is in the opposite direction than presented in Fig. 1. The stiffener imperfections are given as a value c_0 in Table 2. The corrosion degradation level was measured by the Degree of Degradation – *DoD*, which is considered a percentage of the initial volume of the specimen.

The accelerated corrosion tests have been discussed in detail in Woloszyk et al. (2021b), but some main aspects are given herein. The nine stiffened plates have been subjected to the laboratory indoor accelerated corrosion testing, and the set-up is presented in Fig. 2, left.

Table 1
Mechanical properties (Woloszyk et al., 2020).

Thickness [mm]	Young modulus, E [GPa]	Yield stress, R_e [MPa]	Ultimate tensile stress R_m [MPa]	Total elongation δ [-]
5	197	272	389	0.266
6	196	284	410	0.260
8	199	361	465	0.219

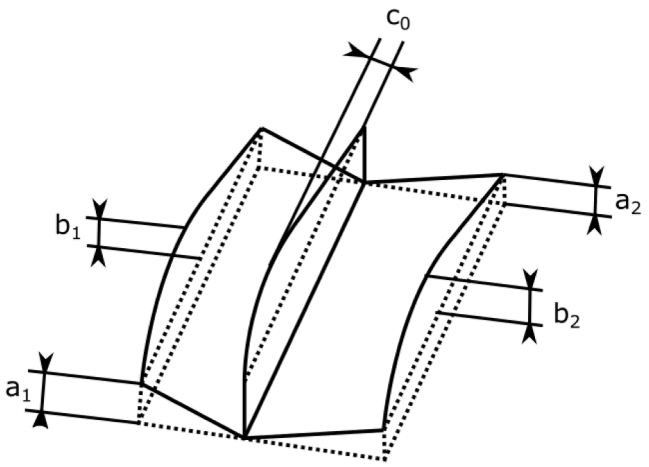

Fig. 1. Initial imperfections (Woloszyk et al., 2021a).

Table 2
Initial imperfections of corroded stiffened plates (Woloszyk et al., 2021a).

Thickness [mm]	No	DoD [%]	a_1 [mm]	a_2 [mm]	b_1 [mm]	b_2 [mm]	c_0 [mm]
5	1.5	7.2	2.37	5.19	−7.98	5.37	1.19
	2.5	21.1	3.45	3.05	−8.91	9.02	3.35
	3.5	0	2.78	3.37	−6.98	4.49	2.95
	4.5	13.6	2.33	3.49	−5.34	3.95	0.00
6	1.6	13.5	3.73	3.66	3.69	−4.10	2.18
	2.6	0	4.01	4.17	3.58	−4.95	0.72
	3.6	20.4	4.62	3.12	2.19	−5.01	0.85
	4.6	6.7	4.36	3.21	0.63	−5.19	0.60
8	1.8	13.8	3.77	5.50	−3.01	−2.43	0.22
	2.8	6.9	4.31	5.07	−0.25	−0.11	0.44
	3.8	22.3	4.25	4.73	1.39	1.46	0.77
	4.8	0	4.61	5.05	−1.01	−1.07	0.45

The corrosion degradation has been controlled by generating appropriate: temperature (heaters), water circulation (circulation pumps) and aeration (aeration pump with linear diffuser). The testing tank with the placed specimens (without water inside) is presented in Fig. 2, right. The main advantage of the performed testing was that it avoided using the acceleration of corrosion rate by connecting the specimens and water to DC power, and only natural factors were controlled. This led to environmental conditions closer to the real one. It needs to be also noted, that for some period of operation, the structural elements are effectively protected by the coating (usually around 8–10 years (Guedes Soares et al., 2008)). The corrosion degradation control parameter considered in this study is Degree of Degradation, which is estimated based on the thickness measurements, independently of the exploitation time. Thus, the coating was not considered in the present study.

The target degradation levels were established at 7, 14 and 21% of *DoD* for each group of thickness. However, the mass of the specimens was not measured constantly and only with a specified time instance. Additionally, the specimens were cleaned from corrosion products. Thus, the finally achieved degradation levels are given in Table 2.

The examples of corroded specimens are presented in Fig. 3. The thickness distribution of each specimen was measured using an ultrasonic thickness gauge in the grid points, as is visible in Fig. 3. The detailed maps with thickness distributions can be seen in Woloszyk et al. (2021b). The mean value corrosion rate was between 0.75 up to 1.15 mm/year, which shows a significant acceleration of the corrosion degradation process concerning typically observed values in the natural sea corrosion environment (Zayed et al., 2018).

The specimens were tested using compressive loading using a hydraulic machine, clamped in the shorter edges using specially designed supports (Woloszyk and Garbatov, 2019), as presented in Fig. 4. The tests were conducted in the Laboratory of Marine Structures at the Gdansk University of Technology. The experimental set-up was already introduced in Woloszyk et al. (2021c), where the effectiveness of the supporting structure has been verified by employing experimental and numerical analysis. It has been shown that the specimens behaved almost entirely clamped, which was the primary aim of the designed supports. The intact specimens have been tested, as described in Woloszyk et al. (2020). The mid-cross-section's lateral deflection in the middle of the specimen and strains were measured using displacement transducers and strain gauges, respectively. For corroded specimens, the strain gauges were not used to avoid destroying the corroded surfaces. The proper application of strain gauges requires a precise grinding of the surfaces in the installation regions. The strain distribution analysis was used to validate the numerical model for intact specimens, as reported in Woloszyk et al. (2020). Thus, overall buckling behaviour and the impact of boundary conditions were captured. To distinguish the possible impact of uneven thickness distribution, detailed thickness measurements were performed, as already indicated. Additionally, the possible asymmetric behaviour of specimens due to the unfair thickness distribution was more important, and additional displacement gauges were placed in the side edges of the specimens. The distribution of the displacement transducers for testing corroded specimens is presented in Fig. 4.

The failure mode could also be distinguished by measuring three

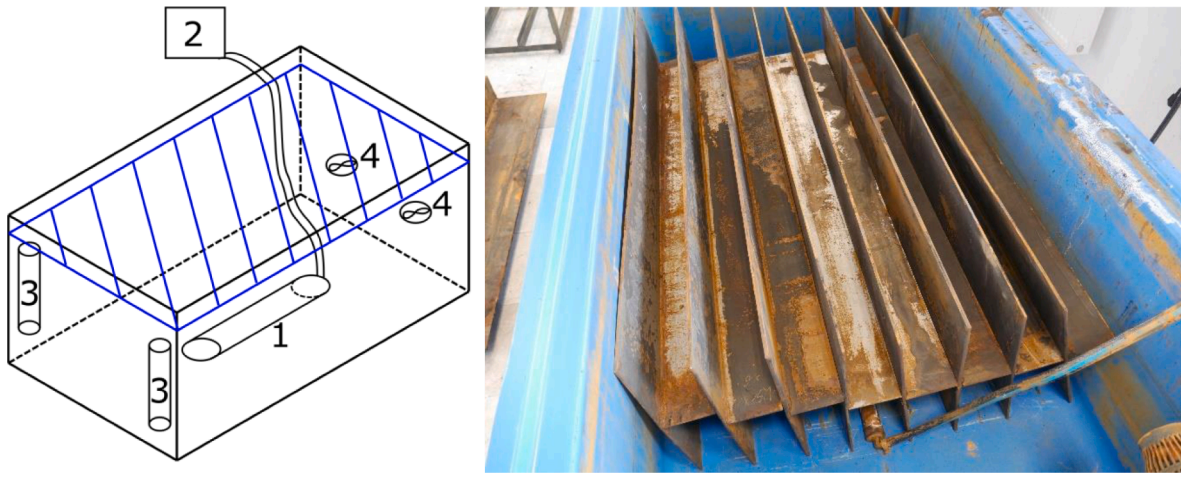

Fig. 2. Corrosion test tank (Woloszyk et al., 2021b) (1- linear diffuser, 2 – aeration pump, 3 - heaters, 4 – circulation pumps) (left) and corrosion tank with placed specimens (right).

Fig. 3. Corroded stiffened plates: 2.5 mm (left); 4.6 mm (mid); 3.8 mm (right) (Woloszyk et al., 2021b).

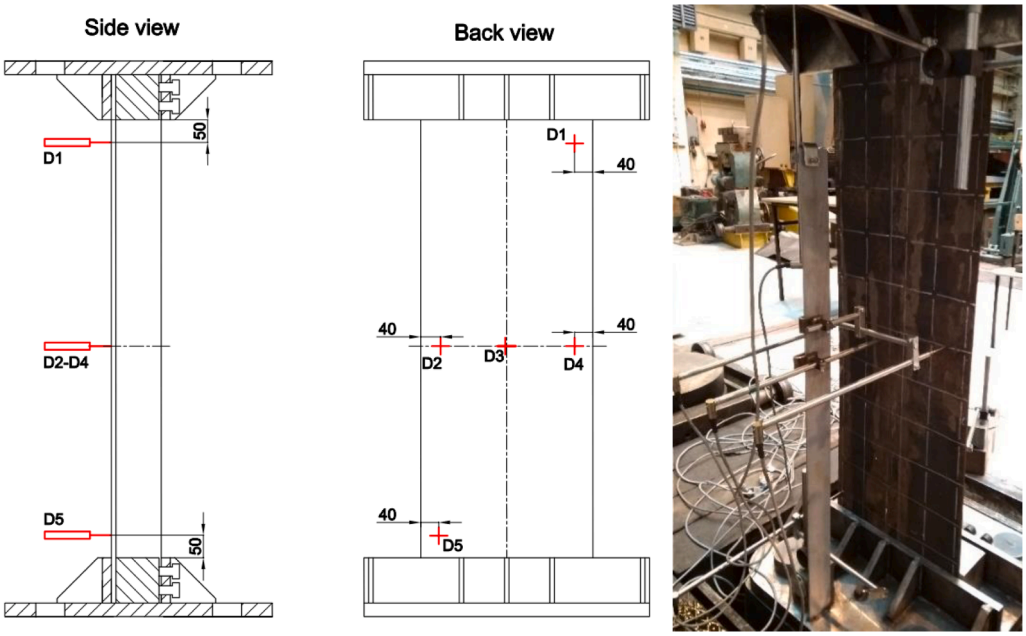

Fig. 4. Distribution of displacement transducers.

lateral displacements in the mid-cross-section (gauges D2 – D4). In terms of gauges D1 and D5, there were left to monitor the near-support displacement as an additional validation input for the effectiveness of the proposed supporting system. The standard testing machine, equipped with a hydraulic pressure system allowing a maximum load of compression of 4,000 kN and tension of 2,000 kN, was used in the experimental testing. The main output from the performed tests was the relation between compressive force and longitudinal displacement for each specimen.

3. Strength assessment

3.1. Compressive force

The obtained ultimate compressive forces are presented in Table 3. Additionally, the compressive forces for intact specimens from a previous study (Woloszyk et al., 2020) were reported too. As indicated in Section 3.3, the observed failure modes were quite similar for both intact and corroded stiffened plates.

In Fig. 5, the relative decrease of ultimate force concerning initial value depending on the *DoD* level is presented. It can be noticed that the

Table 3
Ultimate force for different thicknesses and DoD.

Thickness [mm]	Ultimate force [kN]			
	Intact	*DoD* = 7%	*DoD* = 14%	*DoD* = 21%
5	380.2	312.5	271.8	210.1
6	552.3	469.3	426.0	278.2
8	953.9	836.6	662.8	532.1

ultimate strength significantly decreases with corrosion development. It is observed that the reduction in the strength is very similar for different thicknesses and follows a linear trend. In the case of the mean value thickness reduction of 21%, the approximately 46% strength reduction has been observed.

Although the plate slenderness will increase with the thickness reduction, the decrease of the ultimate strength is less dramatic if only the thickness reduction impact is considered. To analyse that, the results are compared with the empirical formulation of Paik and Thayamballi (1997) (which was found to predict the ultimate strength of intact stiffened plates with a difference not exceeding 6% (Woloszyk et al., 2020)) (see Fig. 5). It needs to be highlighted, that in Woloszyk et al. (2020), both experiments and non-linear FE simulations of compressed non-corroded stiffened plates were performed and the results were very similar to empirical formulations of Paik and Thayamballi (1997). Thus, it could be considered, that the eventual problem of differences in boundary conditions was already verified for intact specimens. The ultimate strength could be calculated as follows (Paik and Thayamballi (1997)):

$$\frac{\sigma_U}{R_e} = \frac{1}{\sqrt{0.995 + 0.936\lambda^2 + 0.17\beta^2 + 0.188\beta^2\lambda^2 - 0.067\lambda^4}} \quad (1)$$

where:

β is the plate slenderness ratio calculated equal to $b/t\sqrt{R_e/E}$ (b is the plate breadth and t is the plate thickness);

λ is the column slenderness ratio of stiffener with the attached full plating equal to $l/\pi r\sqrt{R_e/E}$ (l is the stiffened plate length, r is the radius of gyration of the stiffened plate cross-section).

The calculated plate slenderness ratios and column slenderness ratios considering the mean reduction of stiffened plate thickness are presented in Table 4.

The empirical formulation results show an approximately 30% decrease in plate strength, which is less than estimated based on the experimental results. Thus, the reduction of mechanical properties (Garbatov et al., 2014b), together with the non-uniform distribution of the thickness in the stiffened plate (Woloszyk et al., 2021b), are the factors that are most likely to contribute to the reduction of the stiffened plate ultimate strength when considering the corrosion degradation. However, future detailed FE analysis is need to be performed to verify this hypothesis. It needs to be highlighted that in the most common approach, only the mean thickness reduction is considered the corrosion degradation impact. For example, it is used in current rules of classification societies (e.g. Common Structural Rules for Bulk Carriers and Oil Tankers (International Association of Classification Societies, 2018)). Thus, the strength prediction is non-conservative in this case.

Additionally, the strength reduction was significantly higher when compared to the specimens corroded electrochemically (Garbatov et al., 2017) (see Fig. 5). The curve presented in Fig. 5 has been established as the regression from experimental points. For that case, the thickness

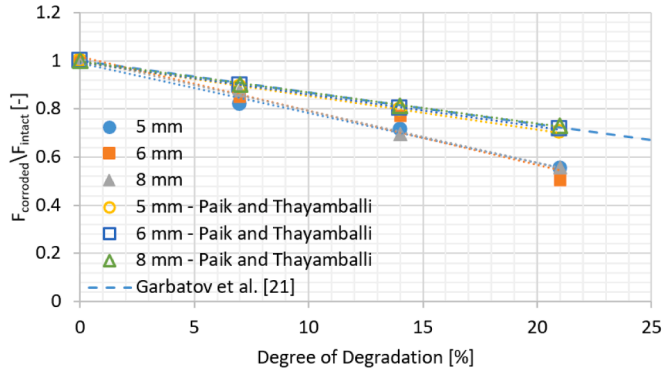

Fig. 5. Relative strength reduction vs degradation level.

Table 4
Plate and column slenderness ratio considering mean loss of thickness.

Initial thickness t [mm]	Slenderness ratio	Degree of Degradation DoD [%]			
		0	7	14	21
5	β [-]	2.97	3.19	3.45	3.76
	λ [-]	0.508	0.509	0.510	0.512
6	β [-]	2.54	2.73	2.95	3.21
	λ [-]	0.516	0.518	0.520	0.521
8	β [-]	2.13	2.29	2.47	2.69
	λ [-]	0.569	0.571	0.574	0.576

variations were not that high, like in current investigations, leading to a decrease of strength of about 30% for a similar degradation level. In fact, for that degradation level, the results were closed to values obtained from the empirical formulation of Paik and Thayamballi (1997).

3.2. Force-displacement relationships

The relationships between longitudinal shortening of the stiffened plates and compressive force were presented in Figs. 6–8. Fig. 6 shows the force-displacement curves for specimens of an initial 5 mm thickness are presented. It can be noted that the curves are similar. At the beginning of the loading process, the slope of the curves is relatively low, resulting from the readjustment of the specimen in the supports. Interestingly, the initial stiffness for non-corroded specimens is lower when compared to corroded ones. This may be the result of non-perfect measurements of the longitudinal displacements. The initial slope is reduced within the range between 7% up to 21% of the degradation level. However, the longitudinal displacement was measured only on the lower support for a non-corroded specimen, which may overestimate this value. In corroded specimens, the difference between the displacements in the lower and upper supports was considered. It is noted that the ultimate strength has been reached for different longitudinal displacements between 3 up to 5 mm. Apart from that, there are no visible significant differences in pre-collapse behaviour. In terms of the post-collapse behaviour, the severely corroded specimens seem to collapse more prominently, which may be seen in the case of a decrease of the response force after the ultimate point is reached. In the case of DoD = 21%, the post-collapse behaviour of the corroded specimen was not traced due to the computer's error that captured the experimental data. Nevertheless, the essential ultimate strength and the pre-collapse stage have been captured.

Fig. 7 shows the force-displacement curves for specimens of an initial thickness of 6 mm. Apart from the initial scatter caused by the initial readjustment of the specimens in the supports (specimens with 14 and 21% of corrosion loss), the force-displacement relationship is quite similar regardless of the degradation level. The ultimate strength is

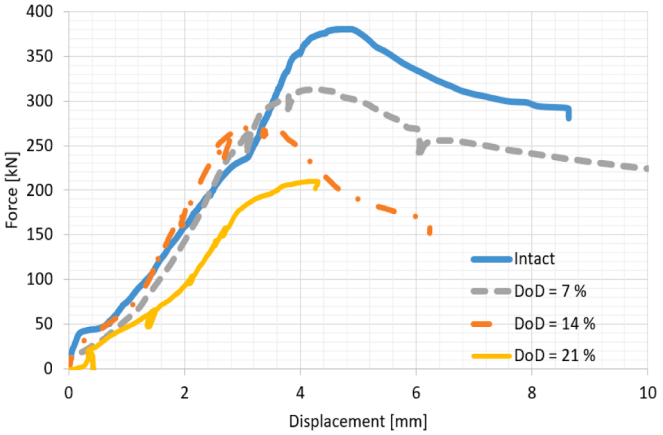

Fig. 6. Force-displacement relationships for 5 mm specimens.

located at a similar point between a 4 and 5 mm longitudinal displacement. The initial slope of the curves decreases with the corrosion development for all specimens of different *DoD*. Both pre-and post-collapse regimes are relatively similar.

The force-displacement curves for 8 mm specimens are presented in Fig. 8. It is noted that the initial stiffness of the specimen was lower with the corrosion degradation growth, which can be seen in terms of the initial slope of the force-displacement relationship. The only irregular behaviour is noted for a specimen with a *DoD* level of 7%, where some severe reduction in the strength in pre-collapse behaviour occurred. Nevertheless, both pre-and post-collapse behaviours were somewhat similar and were not strongly dependent on the corrosion *DoD*. The point of ultimate strength has been reached between 4 mm and 6 mm of the longitudinal displacement.

It could be noted in Figs. 6–8 that force-displacement curves are not continuous in some places. Notably, before reaching ultimate strength, force and displacement dropped and increased again. This may be caused by several reasons, including localised failure and readjustment of the specimen (Woloszyk et al., 2021c), and losing the welding integrity during the incremental loading (see Fig. 9).

3.3. Post-collapse forms

There are several possible failure modes of stiffened plates subjected to uniaxial compressive loading. The primary failure modes are (Yao and Fujikubo, 2016): local plate buckling, lateral-torsional buckling of the stiffener, stiffener tripping and global column buckling. In the case where the stiffeners have sufficient flexural rigidity and little deflection, the plate predominantly buckles. If flexural rigidity will be not sufficient, the stiffener will buckle together with the plate, leading to the overall buckling of the stiffened panel. Finally, there are two modes, where only stiffener buckles. The first one is the lateral-torsional buckling, where the stiffener is rotating about the plate-stiffener connection line. However, for slender stiffeners, such as a flat-bar stiffener, the more localized buckling, like tripping is observed. However, the failure modes could interact, thus one will be the primary reason for failure, but another will occur too.

The post-collapse shapes for 5 mm specimens are presented in Fig. 9. In specimens with *DoD* of 7 and 21%, the collapse has been caused by the local plate buckling followed by stiffener tripping, like the intact specimens. Primarily, the plate buckled locally, which initiated the collapse of the stiffened plate. However, due to the loss of in-plane stiffness, the stiffener also started to buckle in a very localized mode. The cross-section of the highest plastic deformations was away from the mid-length of the specimen due to the uneven distribution of the corroded thickness of the plate and the stiffener for each degradation level. In the case of 5 mm specimens, the regions of high corrosion diminutions were closer to the upper support, which caused a similar position of a critical cross-section. Further, in the specimen with a *DoD* of 14%, the region of high plastic deformations was not that localised and has been more extended along with the specimen, which indicates that the local plate buckling occurred together with the lateral-torsional buckling of the stiffener.

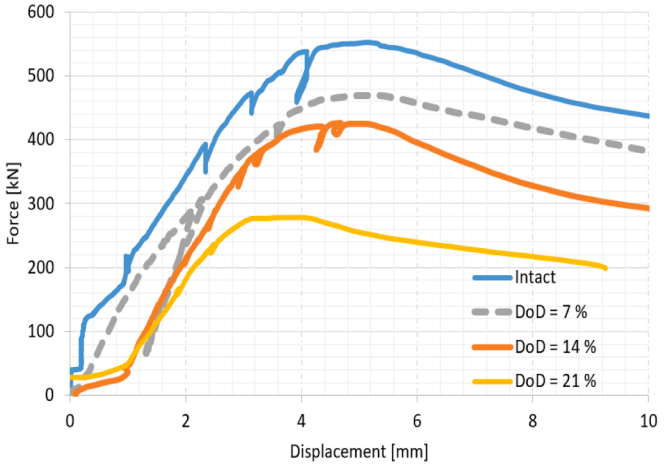

Fig. 7. Force-displacement curves for 6 mm specimens.

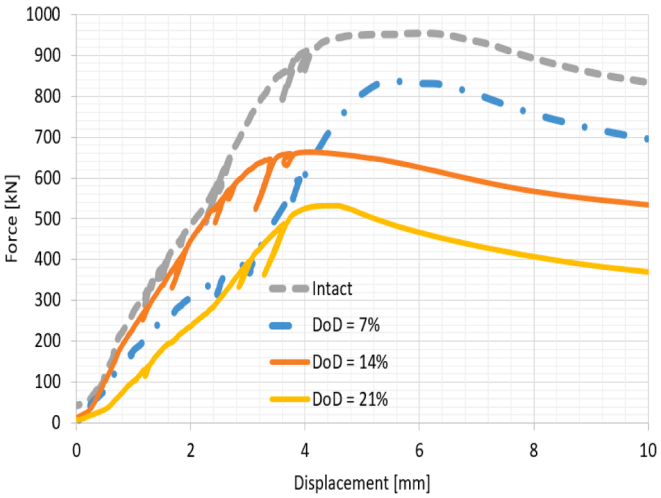

Fig. 8. Force-displacement curves for 8 mm specimens.

The post-collapse shapes for 6 mm specimens are presented in Fig. 10. In the case of *DoD* of 7% and 14%, similarly to previous specimens, the collapse has been caused by local plate buckling followed by stiffener tripping. For those specimens, the regions of highest plastic deformations were obtained away from the middle of the specimen. In the most severe corroded specimen, the local plate buckling was the primary cause of the collapse. However, it was followed by global column buckling which is visible by the significant localised plastic deformations in the middle of the stiffener. These observations are also visible when analysing the measurements of lateral displacements.

Fig. 11 shows the post-collapse shapes of 8 mm stiffened plates. It is noted that the collapsed section in the case of 7% and 21% of *DoD* was almost near the lower support. This was caused due to the high thickness diminutions in that region. The observed failure mode has been the local plate buckling followed by stiffener tripping for all specimens, similarly to other groups of thicknesses. However, for all specimens, some level of global buckling occurred too.

The comparison between the failure modes is presented in Table 5. It is noted that the local plate buckling was the predominant failure mode in all analysed cases. After that, stiffener tripping occurred in many cases. However, in the case of the most severely corroded 6 mm plate thickness specimen, the global buckling was observed afterwards and in the case of the 5 mm specimen with *DoD*=14%, the torsional buckling of stiffener was observed.

The plate slenderness ratio of analysed specimens varies between 2.13 and 3.76, whereas the column slenderness ratio varies between 0.397 and 0.654. By comparing these values with those typically observed in ship structures (Zhang, 2015), the plate slenderness ratio can be considered relatively high, and the column slenderness is within the mean range. Thus, the observed plate buckling mode, as the dominant one, is consistent with the slenderness ratio since the plate slenderness ratio is in general higher in comparison to the column slenderness ratio. Further, since the flat-bar stiffener is in of lower torsional constant with comparison to e.g., T-bar stiffener, the observed stiffener tripping, which became after plate buckling is also justified. It could be noticed that the corrosion degradation (at least within the considered range) will have no impact on the observed failure mode. The first distinction from this rule is the 5 mm specimen with a 14%

Fig. 9. Post-collapse shapes for 5 mm specimens with degradation level of 7% (left), 14% (mid) and 21% (right).

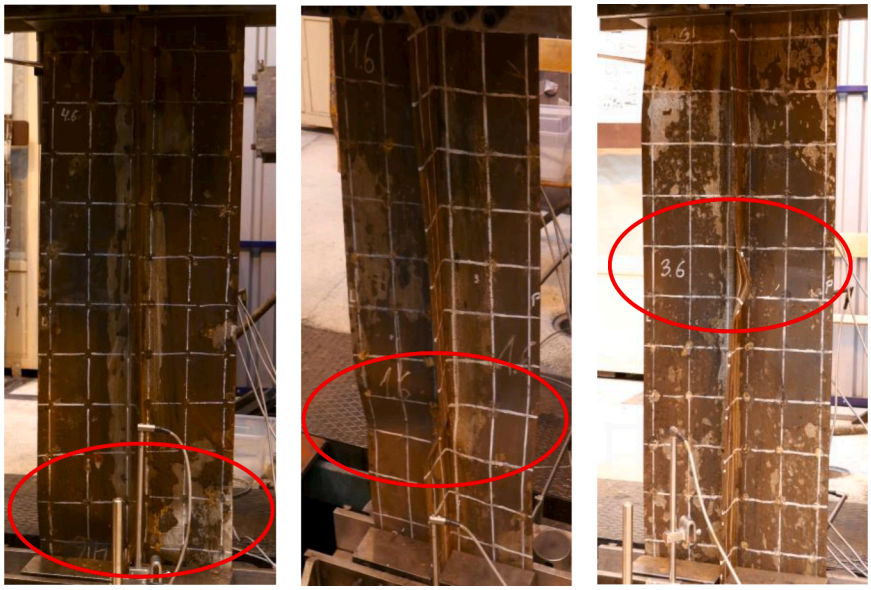

Fig. 10. Post-collapse shapes for 6 mm specimens with *DoD* of 7% (left), 14% (mid) and 21% (right).

degradation level. However, in this case, the stiffener has almost no imperfections at the beginning (see specimen 4.5 in Table 2). This led to more general buckling of the stiffener (torsional buckling) instead of localized tripping. The second deviation from the general observation is the 6 mm specimen with a 21% level of corrosion degradation. In this case, both plate and stiffener initial imperfections were rather similar compared to other specimens in that group of thicknesses. Thus, only an uneven distribution of the thickness due to corrosion degradation is the reason for such deviation.

The stiffened plate region, where the highest plastic deformations occurred, was somewhat away from the middle due to uneven thickness distribution (the regions are marked in red envelopes in Figs. 9–11). In many cases, it was very close to the support. In the case of electrochemically corroded plates (Garbatov et al., 2017), these regions were much closer to the middle cross-section in most cases, even for much higher degradation levels. This was caused by a more uniform thickness distribution (although non-uniform) compared to the present research.

3.4. Lateral displacements

Firstly, the lateral mid-displacements (gauge D3) are compared for each thickness group, as presented in Fig. 12, as a function of the longitudinal shortening of the specimens. The observations of post-collapse shapes for 5 mm specimens are consistent with the measurements of the mid-lateral displacements of the specimens (see Fig. 12, left, top). It is noted that for both curves ($DoD = 7\%$ and $DoD = 21\%$), the lateral mid-displacements increase slightly up to the point of ultimate strength and then decrease due to the significant role of the local buckling. For the curve of $DoD = 14\%$, after the local plate buckling, the lateral-torsional buckling of the stiffener occurred. Thus, the lateral mid-displacement slightly increases after reaching the ultimate point, more significantly than other specimens.

The lateral mid-displacement for 6 mm specimens is given in Fig. 12, right, top. The displacements are consistent with the observed post-collapse shapes, as discussed in the previous section. A significant

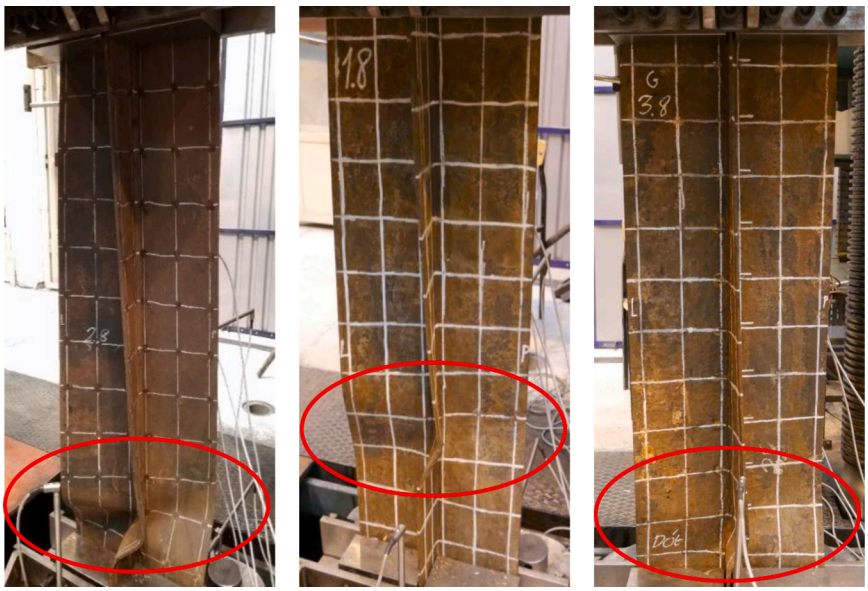

Fig. 11. Post-collapse shapes for 8 mm specimens with degradation level of 7% (left), 14% (mid) and 21% (right).

Table 5
Observed failure modes.

Thickness [mm]	Intact state	*DoD* = 7%	*DoD* = 14%	*DoD* = 21%
5	PB-ST	PB-ST	PB-TB	PB-ST
6	PB-ST	PB-ST	PB-ST	PB-GB
8	PB-ST	PB-ST	PB-ST	PB-ST

Legend: PB – local plate buckling; TB – torsional buckling of stiffener; ST – stiffener tripping; GB – global buckling.

increase in the lateral mid-displacement is noticed in the most severely corroded specimen, indicating that the global buckling contributed to the collapse. For the specimens with a 7 and 14% of degradation level, the local buckling mode was the primary cause of the collapse, leading to a decrease in the mid-displacement after reaching the ultimate strength point.

The observations of the post-collapse of the 8 mm specimens (Fig. 11) are supported by the measurements of lateral mid-displacements (Fig. 12, bottom), where the local plate buckling with a contribution of the global buckling is observed. It is noted that the displacements varieties up to the level of the ultimate point, and there is a slight increase after reaching the highest compressive force.

Figs. 13–15 show the lateral displacements for each specimen separately from gauges D2 – D4. As indicated before, the role of gauges D1 and D5 is only to monitor the clamping supports of the specimens; thus, the results from those measurements are not given herein.

Fig. 13 shows the displacements measured for the 5 mm specimen. It is noted that the plate on both sides of the stiffener buckled locally from

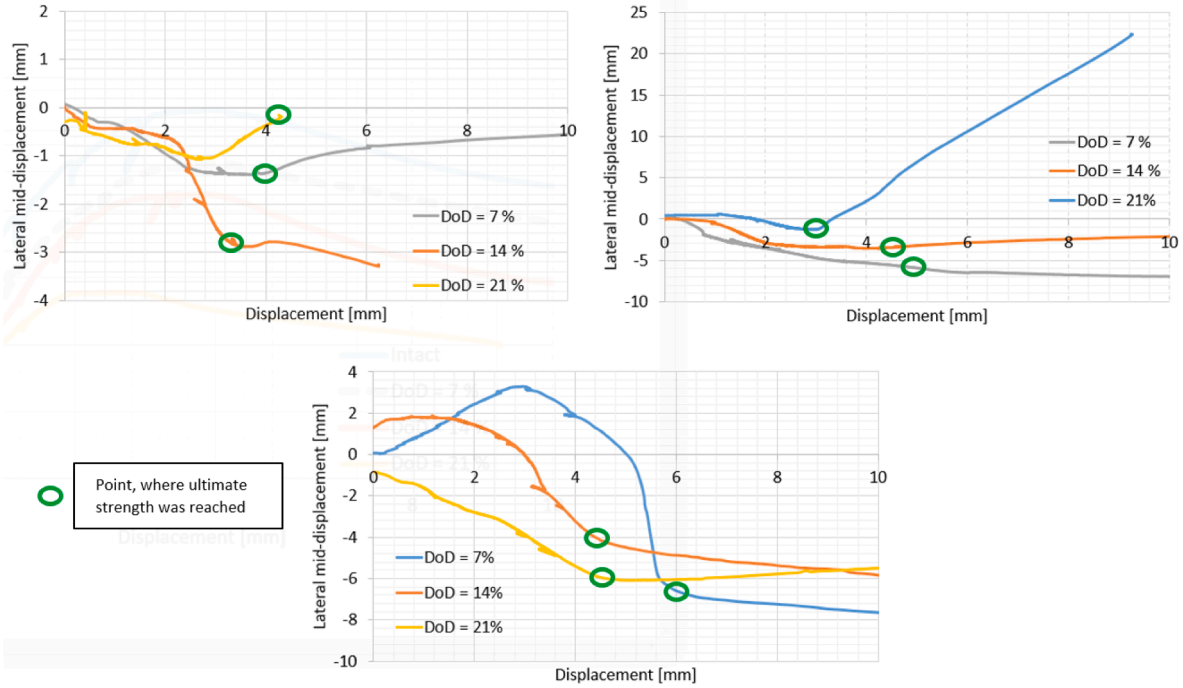

Fig. 12. Lateral mid-displacements vs. longitudinal displacement, corroded specimens of 5 mm (left, top), 6 mm (right, top) and 8 mm (bottom).

the beginning of the loading (the displacements in D2 and D4 are increasing in opposite directions) due to existing initial imperfections (see Table 2). Simultaneously, the stiffener was almost plane until the ultimate strength was reached (displacement D3 was minimal). After getting to the point of maximum compressive force, the displacements on both sides of the plate were relatively constant or even decreased. In the case of the stiffener, for specimens with a 7% and 21% of degradation level, the lateral displacement decreases. However, for a specimen with a 14% level of degradation, due to the existence of lateral-torsional buckling of the stiffener, the mid-lateral displacement increases slightly. The displacements for the most severely corroded plate were not captured in a full range of longitudinal displacement due to the failure of the measuring device.

Fig. 14 presents the lateral displacements measured in 6 mm specimens. In the case of *DoD* equal to 7%, the behaviour is like the 5 mm specimens; thus, the local buckling occurred from the beginning and was mainly observed on both sides of the plate (displacements observed in D2 and D4 gauges). In other specimens, the local plate buckling occurred, and there were very small displacements at the beginning of the loading process. Further, for the most severely corroded stiffened plates, the global buckling after local plate buckling is purely visible since the displacements were growing in the same direction from some point. Thus, it indicates that the mid-cross-section deflected in one direction.

The lateral displacements for 8 mm specimens are presented in Fig. 15. In this case, the local plate buckling was observed after some increments of the loading application. 3, 1 and 0.2 mm of longitudinal displacement were observed for 7, 14 and 21% of *DoD*, respectively. This behaviour is quite understandable since with the corrosion development, the plate slenderness increase, leading to the structure being more prone to buckling. The rest of the observations is somewhat like other specimens. The side-way deflections increase up to the moment when ultimate strength is reached, and then, there are relatively constant.

4. Conclusions

The work analysed experimentally the strength of stiffened plates subjected to marine immersed corrosion made of normal strength steel, considering lower corrosion degradation levels generated by changing the natural corrosion environmental factors.

It was found that the decrease of strength due to corrosion is evident even for lower degradation levels. The ultimate strength may be reduced by almost 50% for the corrosion degradation level of approximately 21%. This level is much higher than specimens corroded electrochemically, where a more uniform thickness distribution is found. Nevertheless, more experimental work is needed to verify this conclusion. Further, compared with some empirical formulations, the mean value corrosion thickness loss is proven to be insufficient in determining the decrease of the stiffened plate strength, which changes both plate and column slenderness ratios. Therefore, more advanced models for design need to be developed to account for the complexity of the corrosion degradation phenomena, accounting for corrosion thickness distribution, type of corrosion degradation and corrosion environmental conditions where the structural components are located.

The corrosion degradation also caused a decrease in the stiffness of stiffened plates since, in most cases, the slope of the force-displacement curve was reduced for more degraded plates. The uneven thickness distribution within the specimens had an impact on the post-collapse regime. In the case of intact specimens, the cross-section where the highest deflections occurred was in the middle of the specimen. However, for corroded specimens, it was more related to the local decrease of the plate thickness. Thus, for some stiffened plates, the highest deflections were observed even very close to the supports.

The primary failure mode observed was the local plate buckling and was followed by stiffener tripping in most cases. However, for selected cases, additional failure modes were observed (i.e., global buckling and torsional buckling of stiffener). This is consistent with the buckling for relatively low column slenderness ratios, there was a considerable high plate slenderness ratio. Thus, the corrosion has rather no impact on the observed failure mode. Nevertheless, future studies, accounting also for different failure modes should be performed.

The presented work is a part of the project that aims to develop closed-form solutions accounting for the complexity of corrosion degradation phenomena to be easily applied in the design and re-evaluation of ageing marine structures. Similar studies still need to be performed accounting for the specific corrosion environmental conditions, including the cases when the structural components are neighboured simultaneously by different corrosion environments. Notably, there are no studies related to the ultimate strength of plates corroded atmospherically. The presented experimental results will be also used in

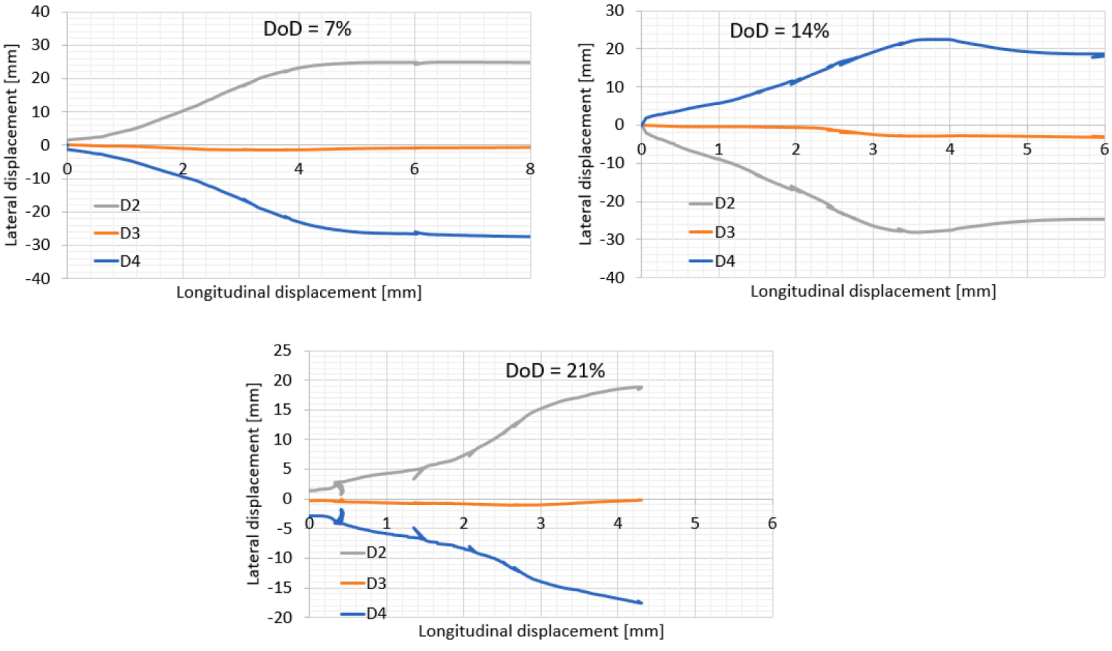

Fig. 13. Lateral displacements in corroded specimens of 5 mm: 7% of *DoD* (left, top), 14% of *DoD* (right, top) and 21% of DoD (bottom).

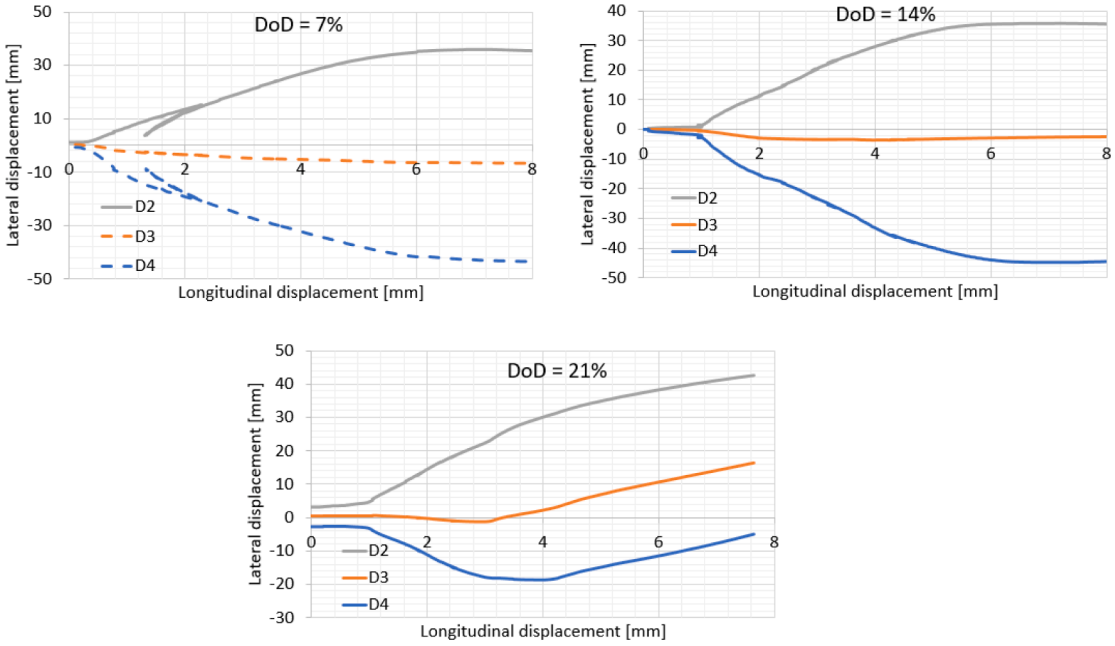

Fig. 14. Lateral displacements in corroded specimens of 6 mm: 7% of *DoD* (left, top), 14% of *DoD* (right, top) and 21% of *DoD* (bottom).

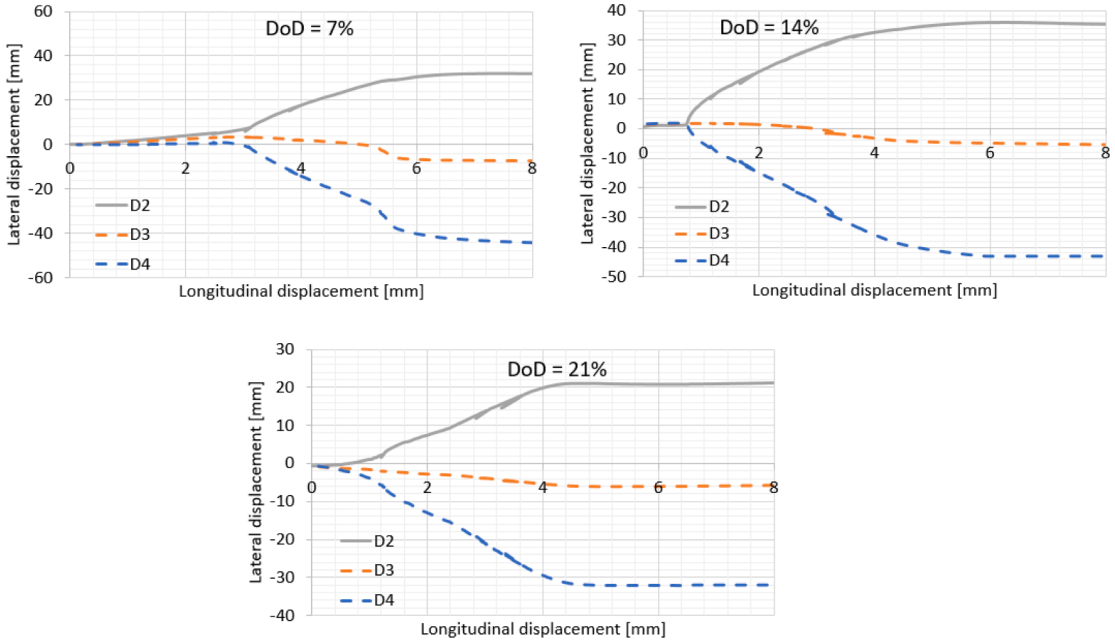

Fig. 15. Lateral displacements in corroded specimens of 8 mm: 7% of *DoD* (left, top), 14% of *DoD* (right, top) and 21% of *DoD* (bottom).

future studies for the validation of the FE model of compressed corroded stiffened plates, accounting for the effect of non-uniform thickness loss and reduction of mechanical properties. Thus, further studies related to numerical modelling and fast approaches are carried out.

CRediT authorship contribution statement

Krzysztof Woloszyk: Conceptualization, Methodology, Formal analysis, Investigation, Writing – original draft, Writing – review & editing. **Yordan Garbatov:** Conceptualization, Methodology, Writing – original draft, Writing – review & editing. **Jakub Kowalski:** Investigation.

Declaration of Competing Interest

The authors declare that they have no known competing financial interests or personal relationships that could have appeared to influence the work reported in this paper.

Acknowledgments

This research was funded by The National Science Centre, Poland (Grant No. 2018/31/N/ST8/02380, entitled "Experimental and numerical investigations of progressive collapse of ageing structures exposed to corrosion and locked cracks").

The first author greatly acknowledges the support of the Foundation

for Polish Science (FNP).

References

Bai, Y., Jin, W.L., 2016. Reassessment of Jacket Structure, in: Marine Structural Design. Elsevier, pp. 875–889. https://doi.org/10.1016/B978-0-08-099997-5.00047-2.

Garbatov, Y., Guedes Soares, C., Parunov, J., 2014a. Fatigue strength experiments of corroded small scale steel specimens. Int. J. Fatigue 59, 137–144. https://doi.org/10.1016/j.ijfatigue.2013.09.005.

Garbatov, Y., Guedes Soares, C., Parunov, J., Kodvanj, J., 2014b. Tensile strength assessment of corroded small scale specimens. Corros. Sci. 85, 296–303. https://doi.org/10.1016/j.corsci.2014.04.031.

Garbatov, Y., Saad-Eldeen, S., Guedes Soares, C., 2015. Hull girder ultimate strength assessment based on experimental results and the dimensional theory. Eng. Struct. 100, 742–750. https://doi.org/10.1016/j.engstruct.2015.06.003.

Garbatov, Y., Tekgoz, M., Guedes Soares, C., 2017. Experimental and numerical strength assessment of stiffened plates subjected to severe non-uniform corrosion degradation and compressive load. Ships Offshore Struct. 12, 461–473. https://doi.org/10.1080/17445302.2016.1173807.

Guedes Soares, C., Garbatov, Y., 1999. Reliability of maintained, corrosion protected plates subjected to non-linear corrosion and compressive loads. Mar. Struct. 12, 425–445. https://doi.org/10.1016/S0951-8339(99)00028-3.

Guedes Soares, C., Garbatov, Y., Zayed, A., Wang, G., 2008. Corrosion wastage model for ship crude oil tanks. Corros. Sci. 50, 3095–3106. https://doi.org/10.1016/j.corsci.2008.08.035.

International Association of Classification Societies, 2018. Common Structural Rules (BC & OT). International Association of Classification Societies.

Kim, D.K., Park, D.K., Kim, J.H., Kim, S.J., Kim, B.J., Seo, J.K., Paik, J.K., 2012a. Effect of corrosion on the ultimate strength of double hull oil tankers - part I: stiffened panels. Struct. Eng. Mech. 42, 507–530. https://doi.org/10.12989/sem.2012.42.4.507.

Kim, D.K., Park, D.K., Park, D.H., Kim, H.B., Kim, B.J., Seo, J.K., Paik, J.K., 2012b. Effect of corrosion on the ultimate strength of double hull oil tankers - part II: hull girders. Struct. Eng. Mech. 42, 531–549. https://doi.org/10.12989/sem.2012.42.4.531.

Kodvanj, J., Garbatov, Y., Guedes Soares, C., Parunov, J., 2021. Numerical analysis of stress concentration in non-uniformly corroded small-scale specimens. J. Mar. Sci. Appl. 20, 1–9.

Mateus, A., Witz, J., 1998. On the post-buckling of corroded steel plates used in marine structures. Trans. RINA 140, 165–183.

Melchers, R.E., 2008. Development of new applied models for steel corrosion in marine applications including shipping. Ships Offshore Struct. 3, 135–144. https://doi.org/10.1080/17445300701799851.

Mohammad, Z.H., Nouri, E., Khedmati, M.R., Roshanali, M.M., 2010. Degradation of the compressive strength of unstiffened/stiffened steel plates due to both sides randomly distributed corrosion wastage. Lat. Am. J. Solids Struct. 7, 335–367. https://doi.org/10.1590/S1679-78252010000300006.

Domzalicki, P., Skalski, I., Guedes Soares, C., Garbatov, Y., Das, P.K., 2009. Large scale corrosion tests. Analysis and Design of Marine Structures. Taylor & Francis Group, pp. 193–198.

Paik, J.K., Thayamballi, A.K., 1997. Empirical formulation for predicting the ultimate compressive strength of stiffened panels. In: Proceedings of the International Offshore and Polar Engineering Conference.

Rahbar-Ranji, A., 2012. Ultimate strength of corroded steel plates with irregular surfaces under in-plane compression. Ocean Eng. 54, 261–269. https://doi.org/10.1016/j.oceaneng.2012.07.030.

Reza Khedmati, M., Mahdi Roshanali, M., Mohammad Esmaeil Nouri, Z.H., 2011. Strength of steel plates with both-sides randomly distributed with corrosion wastage under uniaxial compression. Thin Walled Struct. 49, 325–342. https://doi.org/10.1016/j.tws.2010.10.002.

Saad-Eldeen, S., Garbatov, Y., Guedes Soares, C., 2014. Strength assessment of a severely corroded box girder subjected to bending moment. J. Constr. Steel Res. 92, 90–102. https://doi.org/10.1016/j.jcsr.2013.09.010.

Saad-Eldeen, S., Garbatov, Y., Guedes Soares, C., 2013. Ultimate strength assessment of corroded box girders. Ocean Eng. 58, 35–47. https://doi.org/10.1016/j.oceaneng.2012.09.019.

Saad-Eldeen, S., Garbatov, Y., Guedes Soares, C., 2011. Experimental assessment of the ultimate strength of a box girder subjected to severe corrosion. Mar. Struct. 24, 338–357. https://doi.org/10.1016/j.marstruc.2011.05.002.

Tekgoz, M., Garbatov, Y., Guedes Soares, C., 2020. Review of ultimate strength assessment of ageing and damaged ship structures. J. Mar. Sci. Appl. 19, 512–533.

Vu, V.T., Dong, D.T., 2020. Hull girder ultimate strength assessment considering local corrosion. J. Mar. Sci. Appl. 19, 693–704. https://doi.org/10.1007/s11804-020-00169-9.

Vu Van, T., Yang, P., 2017. Effect of corrosion on the ship hull of a double hull very large crude oil carrier. J. Mar. Sci. Appl. 16, 334–343. https://doi.org/10.1007/s11804-017-1425-7.

Wang, G., Boon, B., Brennan, F.P., Garbatov, Y., Ji, C., Parunov, J., Rahman, T.A., Rizzo, C., Rouhan, A., Shin, C.H., Yamamoto, N., Jang, C.D., Hong, S.Y., 2009. Committee V.6 Condition assessment of aging ships and offshore structures. In: Proceedings of the 17th International Ship and Offshore Structures Congress (ISSC2009), pp. 309–365. Seoul National University, Seul.

Wang, Y., Wharton, J.A., Shenoi, R.A., 2014. Ultimate strength analysis of aged steel-plated structures exposed to marine corrosion damage: a review. Corros. Sci. 86, 42–60. https://doi.org/10.1016/j.corsci.2014.04.043.

Wang, Y., Xu, S., Wang, H., Li, A., 2017. Predicting the residual strength and deformability of corroded steel plate based on the corrosion morphology. Constr. Build. Mater. 152, 777–793. https://doi.org/10.1016/j.conbuildmat.2017.07.035.

Woloszyk, K., Bielski, P.M., Garbatov, Y., Mikulski, T., 2021a. Photogrammetry image-based approach for imperfect structure modelling and FE analysis. Ocean Eng. 223, 108665 https://doi.org/10.1016/j.oceaneng.2021.108665.

Woloszyk, K., Garbatov, Y., Guedes Soares, C., Santos, T.A., 2021. Accelerated large scale test set-up design in natural corrosion marine environment. Developments in Maritime Technology and Engineering. CRC Press, London, pp. 517–524. https://doi.org/10.1201/9781003216582-58.

Woloszyk K., Garbatov Y., 2020a. An enhanced method in predicting tensile behaviour of corroded thick steel plate specimens by using random field approach. Ocean Eng. 213, 107803. 10.1016/j.oceaneng.2020.107803.

Woloszyk, K., Garbatov, Y., 2020b. Random field modelling of mechanical behaviour of corroded thin steel plate specimens. Eng. Struct. 212, 110544 https://doi.org/10.1016/j.engstruct.2020.110544.

Woloszyk, K., Garbatov, Y., Georgiev, P., Soares, C.G., 2019. FE analysis of support-specimen interaction of compressive experimental test. Sustainable Development and Innovations in Marine Technologies. CRC Press, pp. 423–428. https://doi.org/10.1201/9780367810085-56.

Woloszyk, K., Garbatov, Y., Kowalski, J., 2021b. Indoor accelerated controlled corrosion degradation test of small- and large-scale specimens. Ocean Eng. 241, 110039 https://doi.org/10.1016/j.oceaneng.2021.110039.

Woloszyk, K., Garbatov, Y., Kowalski, J., Samson, L., 2021c. Numerical and experimental study on effect of boundary conditions during testing of stiffened plates subjected to compressive loads. Eng. Struct. 235, 112027 https://doi.org/10.1016/j.engstruct.2021.112027.

Woloszyk, K., Garbatov, Y., Kowalski, J., Samson, L., 2020. Experimental and numerical investigations of ultimate strength of imperfect stiffened plates of different slenderness. Polish Marit. Res. 27, 120–129.

Woloszyk, K., Kahsin, M., Garbatov, Y., 2018. Numerical assessment of ultimate strength of severe corroded stiffened plates. Eng. Struct. 168, 346–354. https://doi.org/10.1016/j.engstruct.2018.04.085.

Xiao, L., Peng, J., Zhang, J., Ma, Y., Cai, C.S., 2020. Comparative assessment of mechanical properties of HPS between electrochemical corrosion and spray corrosion. Constr. Build. Mater. 237, 117735 https://doi.org/10.1016/j.conbuildmat.2019.117735.

Yao, T., Fujikubo, M., 2016. Buckling and Ultimate Strength of Ship and Ship-Like Floating Structures. Elsevier.

Yuan, Y., Ji, Y., Shah, S., 2007. Comparison of two accelerated corrosion techniques for concrete structures. ACI Struct. J. 104, 344–347. https://doi.org/10.14359/18624.

Zayed, A., Garbatov, Y., Guedes Soares, C., 2018. Corrosion degradation of ship hull steel plates accounting for local environmental conditions. Ocean Eng. 163, 299–306. https://doi.org/10.1016/j.oceaneng.2018.05.047.

Zhang, D., Gao, X., Su, G., Du, L., Liu, Z., Hu, J., 2017. Corrosion behavior of low-C medium-Mn steel in simulated marine immersion and splash zone environment. J. Mater. Eng. Perform. 26, 2599–2607.

Zhang, S., 2015. A review and study on ultimate strength of steel plates and stiffened panels in axial compression. Ships Offshore Struct. 1–11. https://doi.org/10.1080/17445302.2014.992610.